SEMARAK ILMU PUBLISHING

Semarak Journal of Thermal-Fluid Engineering

Journal homepage:
https://semarakilmu.my/index.php/sjotfe/index
ISSN: 3030-6639

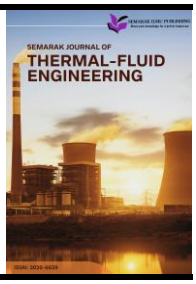

Pressure Drop Analysis of Laminar vs Turbulent Flow in a Straight Pipe

Ahmad Danial Ahmad Junaidi[1,*]

[1] Department of Mechanical Engineering, Faculty of Mechanical Engineering and Manufacturing, University Tun Hussein Onn Malaysia, 86400 Batu Pahat, Johor, Malaysia

ARTICLE INFO

Article history:
Received 15 October 2025
Received in revised form 12 December 2025
Accepted 16 December 2025
Available online 21 December 2025

Keywords:
Laminar flow; turbulence flow; pressure drop

ABSTRACT

Pipelines are commonly used in industrial systems to transport fluids, and their performance is strongly affected by pressure losses that occur along the pipe. These losses depend greatly on the flow regime and the pipe diameter, especially when comparing laminar and turbulent conditions. Although many studies have investigated pipe-flow behaviour, limited attention has been given to how diameter changes influence pressure drop when both laminar and turbulent flows are analysed under the same conditions. In this study, this gap was addressed by examining how three pipe diameters (0.0254 m, 0.0508 m, and 0.0762 m) behave under two different flow regimes using Computational Fluid Dynamics (CFD). Simulations were performed in ANSYS Fluent, where laminar flow was modelled at 0.02 m/s and turbulent flow at 0.3 m/s using the realizable k–ε turbulence model. From the results, it was observed that the smallest pipe experienced the steepest pressure drop in both regimes, with turbulent pressure losses more than four times higher than in laminar flow due to stronger wall shear and intense momentum mixing. In contrast, the larger pipes showed slower pressure decay, smoother flow patterns, and only minor differences between laminar and turbulent conditions. Through this analysis, useful insights were provided for improving the design of straight-pipe systems, where selecting an appropriate diameter can reduce energy losses, improve flow efficiency, and enhance the overall performance of fluid transport operations.

1. Introduction

Internal pipe flow is a fundamental topic in engineering because pressure drop directly influences pumping power, energy efficiency, and overall system performance in fluid transport systems. The behaviour of pressure loss differs significantly between laminar and turbulent flow, and this difference becomes more pronounced when pipe diameter changes. In this study, three standard pipe sizes 0.0254 m diameter,0.0508 m diameter and 0.0762 m pipe are selected based on dimensions reported in past research literature [1]. Although theoretical equations can accurately predict pressure drop for simple single-diameter cases, they cannot fully capture detailed behaviour when comparing multiple diameters across both laminar and turbulent regimes under identical flow

* *Corresponding author.*
E-mail address: dd220062@student.uthm.edu.my

https://doi.org/10.37934/sjotfe.7.1.2537a

conditions. As a result, a clear CFD-based comparison of pressure drop across these three pipe sizes remains limited in the existing literature.

To address this gap, this study employs Computational Fluid Dynamics (CFD) to simulate internal pipe flow and evaluate pressure drop characteristics. The governing Navier–Stokes equations are discretized using the Finite Volume Method (FVM), with the SIMPLE/SIMPLEC scheme applied for pressure–velocity coupling. Near-wall mesh refinement is used to accurately capture wall shear stress and frictional effects. For turbulent simulations, widely accepted Reynolds-Averaged Navier–Stokes (RANS) turbulence models namely the standard k–ε, realizable k–ε, and k–ω SST models are employed. These models are extensively validated for predicting pressure drop and mean-flow behaviour in internal pipe flows and remain practical alternatives when Direct Numerical Simulation (DNS) is computationally infeasible [2,3]. Recent studies comparing these RANS closures against experimental and high-fidelity data confirm that they reliably capture friction losses and velocity profiles in straight-pipe and duct-type geometries when appropriate wall treatment and mesh quality are applied [2,3].

Recent high-fidelity DNS studies have significantly improved the understanding of turbulent pipe flow. A detailed turbulence database for smooth circular pipes at friction Reynolds numbers up to 〖Re〗_T=5200 provides high-resolution mean-velocity and turbulence-intensity statistics that capture large-scale and very-large-scale motions in the outer flow region [4]. These findings show that even high-Reynolds-number pipe flow departs from classical empirical laws, offering robust benchmarks for turbulence-model validation. In addition, the transition from laminar to turbulent pipe flow remains an active research topic. A recent study suggests that transition may be triggered not only by classical kinematic instabilities but also by “material instabilities” arising from modified-viscosity formulations in the Navier–Stokes equations. Their three-dimensional simulations demonstrate that near the transitional Reynolds number, small disturbances can grow into sustained turbulent motion, indicating that additional physical mechanisms may influence transition beyond traditional stability theory. For practical engineering applications, however, RANS turbulence models remain essential because DNS is computationally unrealistic at industrial Reynolds numbers.

Recent comparative studies benchmarking RANS models against higher-fidelity LES/DNS and experimental data in internal and corrugated-pipe flows confirm that calibrated k–ε and k–ω models can reliably predict mean flow and friction factors at a fraction of the computational cost of DNS [5]. Therefore, the aim of this study is to compare laminar and turbulent pressure drop in straight pipes using CFD. The main objectives are to simulate flow for three different pipe diameters, compare pressure drop and velocity profiles between laminar and turbulent regimes, analyse the effect of pipe diameter on pressure loss behaviour, and validate the numerical results against theoretical relations and published research data.

2. Methodology

2.1 Geometry Construction of Straight Pipe

The geometry used in this study consists of a straight circular pipe modelled according to the internal diameters specified in the ANSI commercial pipe sizes standard, ensuring that the simulated configuration represents realistic industrial pipe dimensions. Three pipe sizes were developed for comparison, 0.0254 m, 0.0508 m and 0.0762 m each with an overall length of 1.0 m to allow adequate flow development under both laminar and turbulent regimes [1]. The CAD model was constructed using dimensional data obtained directly from the ANSI specification document [6]. Employing this standard ensures that the pressure-drop predictions produced from the CFD simulations are consistently comparable across all three pipe diameters and remain relevant to real-world

engineering applications. Figure 1 displays the CAD geometry of the three pipes, while Figure 2 illustrates the water flow domain, indicating the inlet and outlet boundaries that define the flow direction within the simulation.

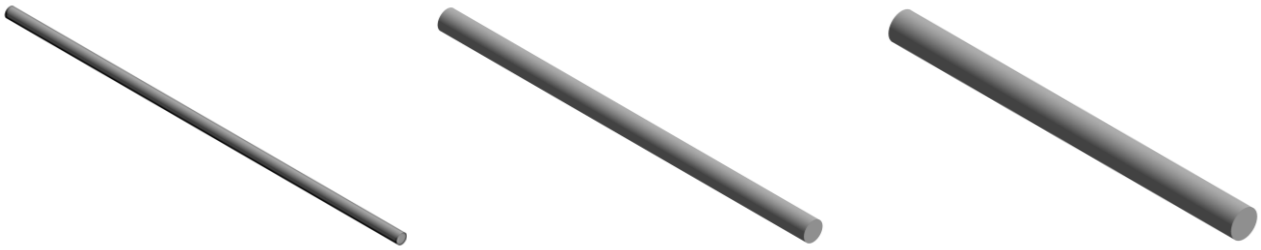

(a) (b) (c)

Fig. 1. The geometry of straight pipe (in diameter) (a) 0.0254 m (b) 0.0508 m (c) 0.0762 m

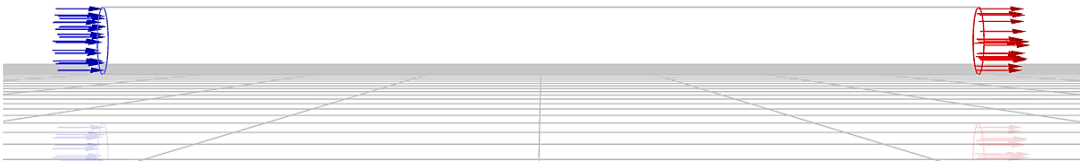

Fig. 2. The geometry of water flow domain showing inlet and outlet flow

2.2 Meshing

The meshing was performed in ANSYS meshing using the Multizone method with a swept (mapped) hexahedral mesh for all three pipe geometries with diameters of 0.0254 m, 0.0508 m, and 0.0762 m. A uniform body sizing control was applied to each pipe to define the element size, which was varied across several mesh configurations to examine the influence of mesh resolution on numerical accuracy. The final selected element size was 0.0036 m, providing a sufficiently refined mesh to capture boundary-layer development along the pipe walls under both laminar and turbulent flow conditions. All three pipe geometries were meshed using the same consistent approach. The mesh quality was evaluated based on skewness and orthogonal quality, and all meshes complied with the quality standards recommended by ANSYS Fluent. The Multizone swept hexahedral mesh applied to the 0.0762 m pipe geometry is shown in Figure 3, demonstrating the structured hexahedral distribution achieved throughout the flow domain.

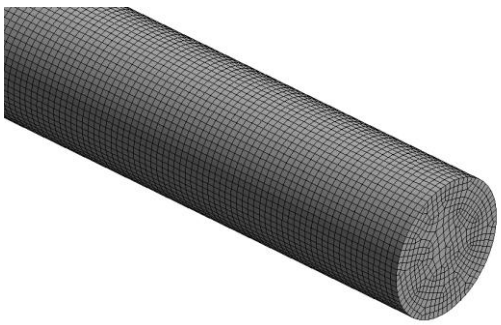

Fig. 3. Multizone swept type Hexa mesh applied to the straight pipe 0.0762 m pipe geometry using Ansys Meshing (element size = 0.0036 m)

2.3 Governing Equation

The fluid flow inside the pipe is modelled using the fundamental conservation equations for mass, momentum, and energy. These equations describe the behaviour of incompressible internal flow for both laminar and turbulent regimes. Since the working fluid is assumed to be incompressible and the flow inside the straight pipe is driven by a pressure gradient, the governing equations simplify accordingly.

2.3.1 Continuity equation

The continuity equation represents the conservation of mass within a control volume. For an incompressible fluid, the density remains constant, and the equation reduces to the requirement that the velocity field must be divergence-free:

$$\nabla.\vec{V} = 0 \tag{1}$$

This implies that the fluid neither accumulates nor loses mass as it flows through the pipe. The continuity equation also ensures that the velocity profile formed along the pipe is consistent with a steady volumetric flow rate.

2.3.2 Momentum equation (Navier-Stokes)

The momentum equation describes the conservation of linear momentum, which accounts for inertial, pressure, viscous, and body forces acting on the fluid. For incompressible flow, the Navier–Stokes equation is written as:

$$\rho\left(\frac{\partial\vec{V}}{\partial t} + \vec{V}.\nabla\vec{V}\right) = -\nabla.\tau - \rho\nabla \tag{2}$$

In fully developed laminar flow inside a smooth pipe, viscous forces dominate the flow behaviour. This leads to the classical Hagen–Poiseuille velocity profile, which has recently been reaffirmed through numerical studies analysing laminar pipe behaviour under varying inlet conditions [5]. The velocity distribution therefore becomes:

$$u(r) = u_{max}\left(1 - \frac{r^2}{R^2}\right) \tag{3}$$

The pressure drop in laminar flow follows:

$$\Delta P = \frac{32\mu \mathrm{LU}}{D^2} \tag{4}$$

For turbulent simulations, a turbulence model (e.g., k–ε, k–ω SST) introduces additional Reynolds stresses, modifying the momentum equation into its Reynolds-Averaged form (RANS):

$$\rho\left(\frac{\partial\bar{u}}{\partial t} + \bar{u}.\nabla\bar{u}\right) = -\nabla\bar{p} + \mu\nabla^2\bar{u} - \nabla.\left(\rho\overline{u'u'}\right) \tag{5}$$

The last term represents the Reynolds stress tensor, which must be modelled using turbulence closures such as k–ε or k–ω SST. Recent studies have shown that RANS turbulence models, when properly calibrated, can reliably predict internal turbulent pipe flow characteristics and friction factors even at moderate to high Reynolds numbers [7,8]. Furthermore, DNS datasets produced in the past few years provide new benchmark data for validating these turbulence models, especially for smooth-wall pipe turbulence and near-wall predictions [9].

2.4 Boundary Condition and Parameter Assumption

The simulation was conducted under both laminar and turbulent flow conditions for water at room temperature (Tables 1 and 2). The flow inside the pipe is modelled as steady-state and incompressible, which is consistent with many internal-flow CFD studies using ANSYS Fluent. For example, in a 2023 double-pipe heat exchanger CFD study, velocity-inlet, pressure-outlet, and no-slip wall conditions under incompressible flow were successfully adopted to simulate pressure and temperature drop behaviour [10]. A no-slip boundary condition is applied at the pipe walls, enforcing zero relative velocity at the surface; this is standard in viscous CFD simulations to accurately capture wall shear stress and friction losses, as seen in recent straight-pipe CFD work [11].

At the inlet, a uniform velocity is prescribed for all three pipe diameters (0.0254 m diameter, 0.0508 m diameter and 0.0762m pipe). For the laminar cases, the inlet velocity magnitude is set to 0.02 m/s, ensuring that the flow remains well within the laminar regime. For the turbulent cases, a higher inlet velocity of 0.3 m/s is applied to produce a sufficiently large Reynolds number for turbulence modelling. Similar to past CFD studies comparing laminar and turbulent flow conditions, this approach allows a clean baseline for evaluating the influence of turbulence modelling on pressure drop [12].

For the turbulent-flow simulations, the standard turbulent modelling approach is used (e.g. a k–ε type model), aligning with recent CFD investigations of internal flow under turbulence conditions [13]. At the outlet, a pressure-outlet boundary condition is set with 0 Pa gauge pressure, serving as a fixed reference plane for static pressure a common and validated configuration in pipe-flow CFD studies [10].

Table 1
Boundary conditions of straight pipe

Boundary type	Condition type
Flow type	Laminar and Turbulent
Inlet	Velocity inlet: 0.02 (laminar) 0.3 (turbulent)
outlet	Pressure outlet: 0 Pa
Wall	No-slip wall
Initialisation	From inlet
Iteration limit	Up to 1000 iteration per case

Table 2
Turbulent flow conditions

Diameter (m)	Velocity	Turbulence intensity	Turbulence mode
0.0254	0.03	5%	$k-\varepsilon$, Realizable
0.0508	0.03	5%	$k-\varepsilon$, Realizable
0.0762	0.03	5%	$k-\varepsilon$, Realizable

2.4 Post-Processing and Flow Analysis Parameters

Post-Processing was carried out using ANSYS Fluent to analyse the internal flow characteristics. Key parameters extracted included velocity magnitude and pressure for laminar meanwhile for analysis for turbulent flow is included with velocity magnitude, turbulence kinetic energy (TKE) and pressure. Contour plots, vector flow diagrams and line graph were generated to visualize the flow development and identify changes in flow behaviour due to variations in diameter and inlet velocity. Additionally, cross sectional profiles were used to examine the uniformity of flow and detect any signs of secondary motion or recirculation zones

3. Results

3.1 Grid Independent Test

In this study, the grid-independence test (GIT) for the 0.0254m pipe was conducted using three mesh densities defined by element sizes of 0.0038 m (coarse), 0.0036 m (medium), and 0.0034 m (fine), and the 0.0036 m mesh was chosen for both laminar and turbulent flow simulations to balance accuracy and computational cost. The element-size refinement increases the number of elements, which enables the simulation to resolve flow gradients especially near walls more accurately, consistent with findings that mesh resolution strongly affects turbulence quantities and flow field accuracy. Figure 4 presents the Grid Independence Test (GIT) for laminar flow in a 0.0254m pipe using three mesh densities (0.0034 m, 0.0036 m, and 0.0038 m). The aim is to confirm that velocity and pressure predictions remain stable across meshes, ensuring the solution is free from discretization effects, following standard CFD refinement procedures [14].

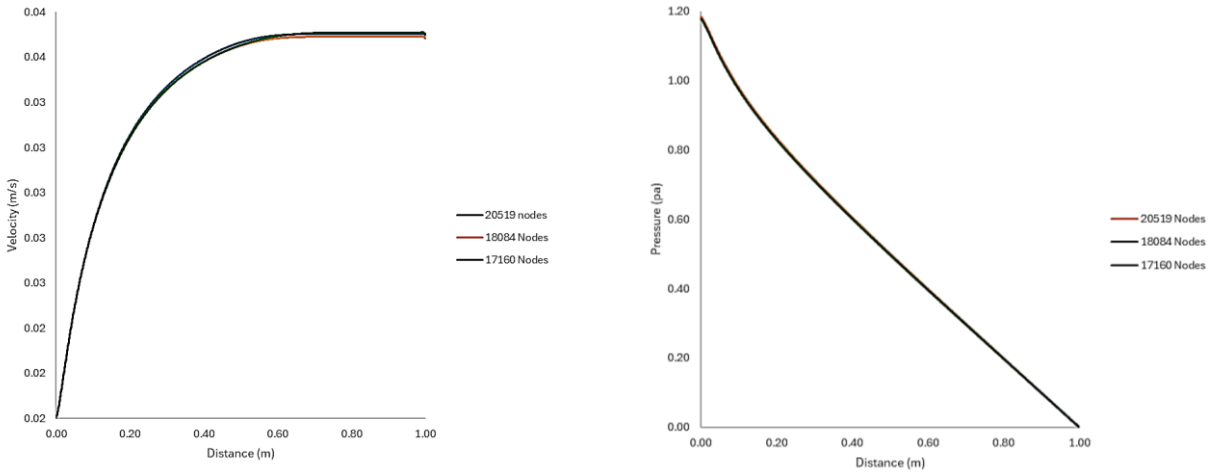

(a) (b)

Fig. 4. The GIT chart of laminar flow (a) Velocity (b) Pressure

Figure 4(a) shows the axial velocity profile, where all meshes begin at 0.020 m/s and follow nearly identical development along the pipe. At x = 4 mm, the meshes differ by less than 0.5% (0.0202–0.0203 m/s), indicating negligible sensitivity to mesh resolution. The steepest gradients appear near the inlet as expected in developing laminar flow, consistent with recent validation findings showing that early regions are most mesh-sensitive but quickly become independent downstream [15]. Figure 4(b) shows the pressure distribution, with all meshes starting at approximately 1.18 Pa and exhibiting the same smooth pressure decay. No visible deviation occurs, even in the entrance region, confirming that refining below 0.0036 m does not significantly change the pressure drop. This aligns with recent

research indicating that laminar internal flow often reaches mesh independence with moderate refinement when near-wall quality is maintained [14]. Given the strong agreement in velocity and pressure, the 0.0036 m mesh was selected as the optimal mesh for laminar analysis. It provides accuracy comparable to the finer mesh without unnecessary computational cost, matching common CFD mesh-selection practices for stable and converged profiles before further analysis [14].

For the turbulent GIT, three meshes (0.0034 m, 0.0036 m, 0.0038 m) were tested. Refinement increased resolution of near-wall turbulence structures, which is important for accurate RANS modelling [14]. In Figure 5, the 0.0034 m and 0.0036 m meshes produced nearly identical velocity, pressure, and TKE curves, while the 0.0038 m mesh showed minor inlet deviations. Since further refinement offered no improvement, the 0.0036 m mesh was chosen for turbulent simulations.

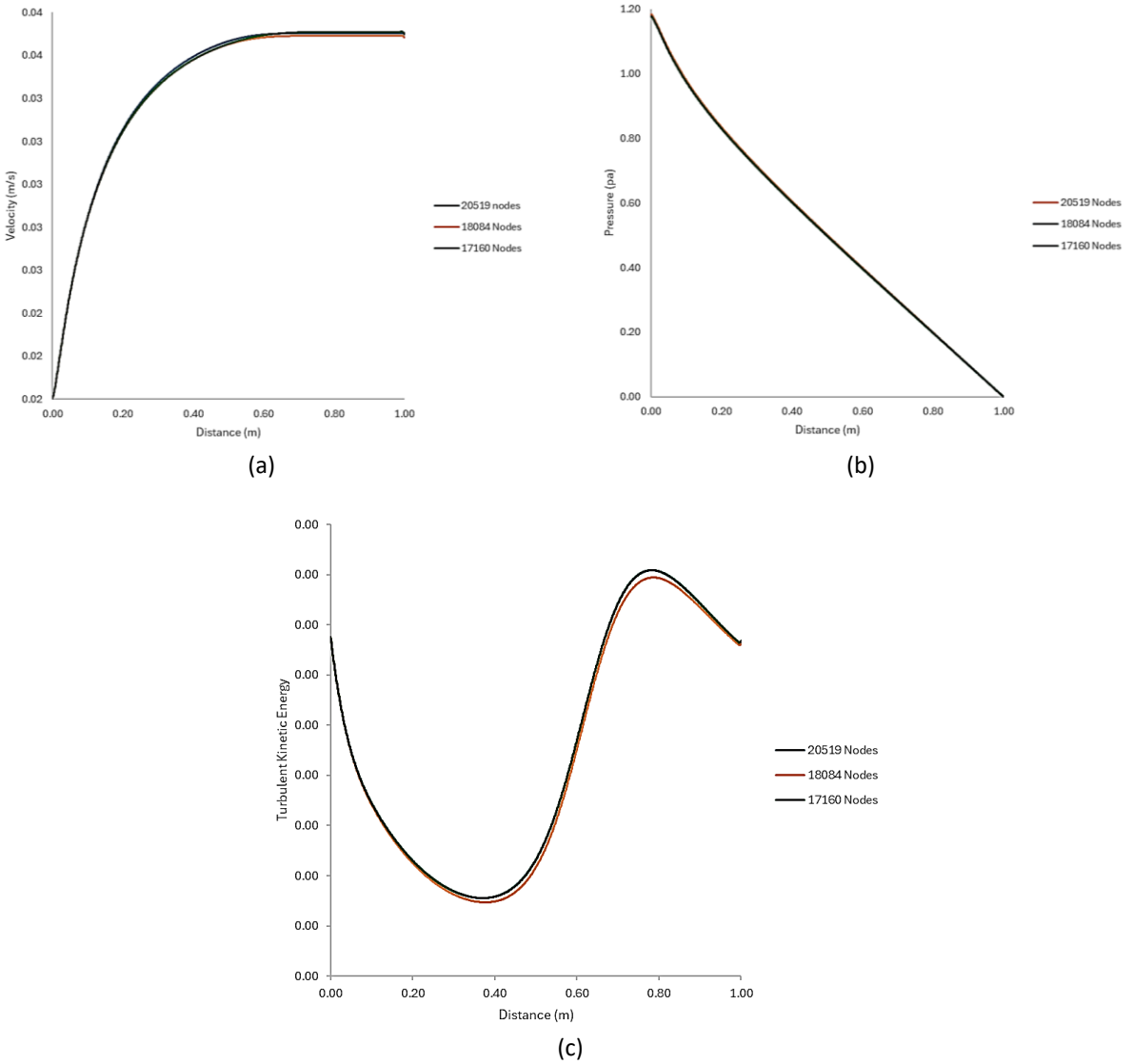

Fig. 5. The GIT chart of turbulent flow (a) Velocity (b) Pressure (c) Turbulent kinetic energy

The extracted numerical results support this decision. The velocity distribution (Figure 5(a)) begins at approximately $0.3000\ m/s\ at\ x\ =\ 0\ m$, gradually increasing to $0.30099\ m/s\ at\ x\ \approx\ 0.001\ m$, and continuing this smooth rise downstream. The coarse mesh displays slightly steeper initial acceleration, but the 0.0036m and 0.0034m meshes produce nearly identical velocity profiles, confirming momentum-field convergence. The pressure distribution (Figure 5(b)) shows a high inlet pressure of $59.63\ Pa\ at\ x\ =\ 0\ m$, dropping slightly to $59.61\ Pa\ at\ x\ =\ 0.001$ m and declining

progressively along the pipe. The similarity between the 0.0036m and 0.0034m pressure gradients indicates that the pressure field is grid independent. In the TKE profile (Figure 5(c)), turbulence intensity starts at $3.38 \times 10^{-4}\, m^2/s^2\, at\, x = 0\, m$, decreasing smoothly to $3.34 \times 10^{-4}\, m^2/s^2\, at\, x \approx 0.001\, m$, before continuing to decay toward the outlet. The coarse mesh slightly overpredicts inlet turbulence ($\approx 3.40 \times 10^{-4}\, m^2/s^2$), whereas the 0.0036m and 0.0034m curves nearly overlap, a trend consistent with previous findings that coarse grids exaggerate TKE due to unresolved turbulent structures [14,16].

Overall, these data confirm that refining from 0.0038 m to 0.0036 m significantly improves solution accuracy, while further refinement to 0.0034m yields negligible benefit. Thus, the 0.0036m element size was selected as the final grid for turbulent simulations, achieving grid-independent results while avoiding unnecessary computational cost aligning with modern CFD best practices [17-19].

3.2 Velocity

Velocity distribution is a fundamental indicator of flow behaviour inside a pipe, allowing clear distinction between laminar and turbulent regimes. In this study, velocity contours are analysed for three different pipe diameters 0.0034 m, 0.0036 m, and 0.0038 m under laminar inlet velocity of 0.02 m/s and turbulent inlet velocity of 0.3 m/s with 5% turbulence intensity using the realizable k–ε model. The velocity contours presented in Figures 6 and 7 illustrate the influence of both flow regime and pipe diameter on internal flow structure.

For the laminar flow case shown in Figure 6, all three pipe diameters exhibit the classical parabolic velocity profile associated with fully developed laminar pipe flow. In the 0.0254 m pipe (Figure 6(a)), the velocity gradient near the wall is very steep due to the strong influence of viscous forces and the small hydraulic diameter, resulting in a high centreline velocity relative to the wall region. This behaviour follows the Hagen–Poiseuille flow theory, where viscous forces dominate and produce a symmetric parabolic velocity distribution [1,19]. When the diameter increases to 0.0508 m (Figure 6(b)), the velocity profile remains parabolic but with a less severe velocity gradient near the wall, indicating reduced wall shear influence. This occurs because increasing the pipe diameter reduces the relative effect of viscous resistance on the core flow [20, 21]. In the 0.0762 m pipe (Figure 6(c)), the velocity contour becomes even more uniform, with the weakest velocity gradient among the three cases. This confirms that larger diameters promote more uniform laminar flow with minimal velocity distortion, as also reported by Marpaung *et al.,* [22].

For the turbulent flow case shown in Figure 7, the velocity contours are significantly different from the laminar results due to the presence of strong turbulent mixing. In the 0.0254 m turbulent pipe (Figure 7(a)), the velocity profile is much flatter across the pipe cross-section compared to the laminar case, indicating intense momentum exchange caused by turbulent eddies. The realizable k–ε model captures this flattening effect, which is a well-known characteristic of turbulent pipe flow [5,8]. Additionally, high velocity gradients are still observed near the wall due to strong wall shear stress. In the 0.0508 m pipe (Figure 7(b)), the velocity field becomes more evenly distributed across the diameter, with a wider uniform core region. The larger diameter reduces the dominance of near-wall turbulence structures, which leads to smoother velocity contours, consistent with findings from Yang *et al.,* [18]. In the 0.0762 m pipe (Figure 7(c)), the velocity distribution is the most uniform among all turbulent cases, indicating that increasing pipe diameter effectively stabilizes the velocity field even under turbulent conditions. This agrees with recent CFD and experimental studies showing that at constant inlet velocity, larger pipes experience weaker velocity distortion due to turbulence [19].

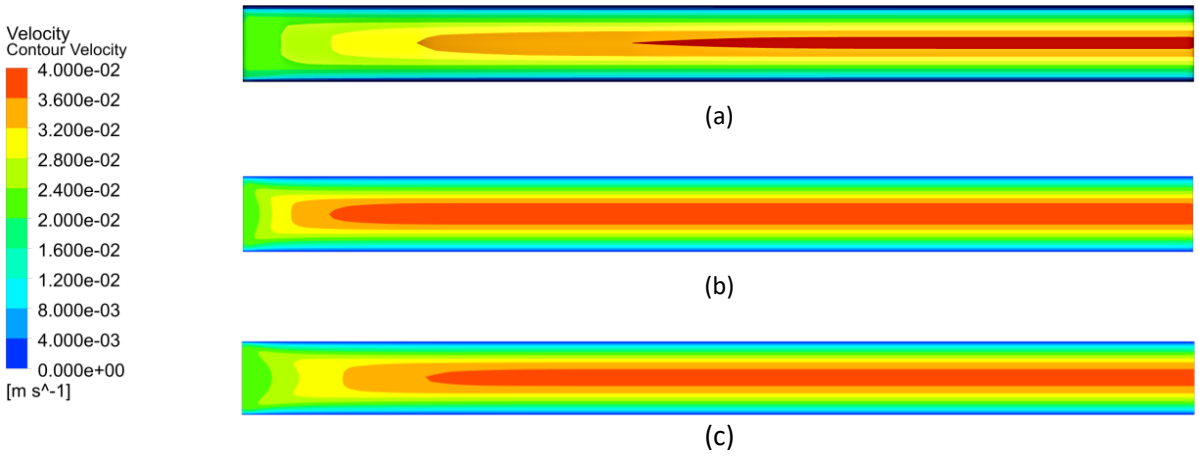

Fig. 6. Velocity contour for laminar flow in diameter pipe (a) 0.0254 m (b) 0.0508 m (c) 0.0762 m

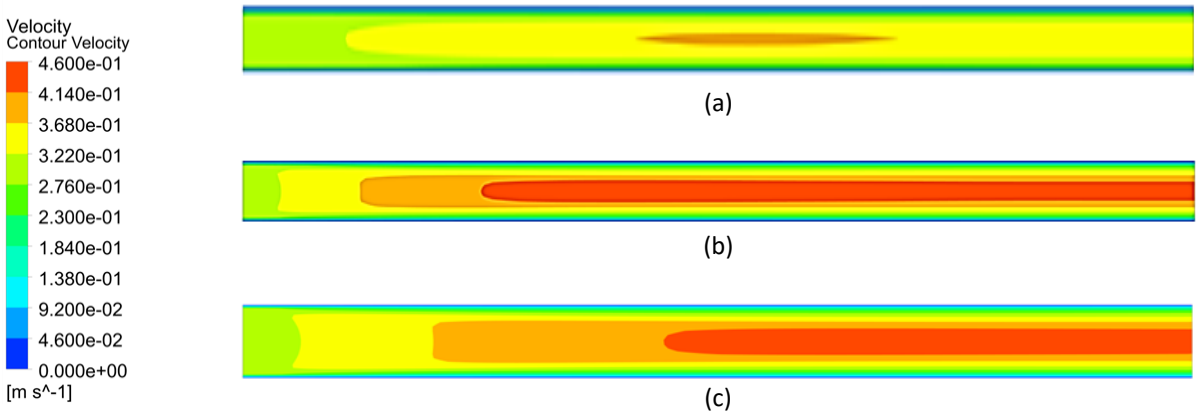

Fig. 7. Velocity contour for turbulent flow in diameter pipe (a) 0.0254 m (b) 0.0508 m (c) 0.0762 m pipe

3.3 Pressure

Pressure distribution is the primary parameter used to evaluate energy loss and flow resistance in internal pipe flows. In this study, pressure contours are analysed for laminar and turbulent flows in three different pipe sizes with a fixed pressure outlet of 0 Pa gauge. The pressure contours for laminar flow are shown in Figure 8, while turbulent pressure contours are shown in Figure 9. These figures clearly demonstrate the combined effects of diameter and flow regime on pressure loss.

For the laminar flow in Figure 8, the 0.0254 m pipe (Figure 8(a)) shows a steep and continuous pressure drop due to strong viscous resistance in the small diameter, which requires higher inlet pressure to maintain the prescribed velocity. As described by the Poiseuille relation, laminar pressure drop is inversely proportional to the square of pipe diameter, making small pipes extremely sensitive to viscous losses [20,21]. In the 0.0508 m pipe (Figure 8(b)), the pressure gradient becomes significantly smoother because the larger hydraulic diameter reduces wall shear stress and flow resistance, consistent with the findings reported by Debtera *et al.,* [12]. For the largest pipe, 0.0762 m (Figure 8(c)), the pressure remains almost uniform along the pipe, indicating very low-pressure loss. This agrees with recent CFD studies showing that laminar pressure losses become negligible in large-diameter pipes under low-velocity conditions [21,12]. Overall, Figures 8 and 9 clearly demonstrate how pipe diameter and flow regime interact to influence pressure-drop behaviour.

For the turbulent flow case in Figure 9, the pressure contours show substantially higher-pressure losses compared to the laminar cases due to additional energy dissipation from turbulence. In the 0.0254 m turbulent pipe (Figure 9(a)), the pressure drop is extremely large, caused by strong wall shear stress and intense turbulent momentum mixing. This behaviour is consistent with turbulent pipe flow theory and DNS-based studies, which show that turbulence significantly amplifies pressure loss, especially in small-diameter pipes [5,20]. In the 0.0508 m turbulent pipe (Figure 9(b)), the pressure gradient is noticeably smaller than in the 0.0254 m case, though still much higher than the laminar condition. The increase in diameter weakens near-wall turbulence production and reduces frictional losses [18,8]. In the 0.0762 m turbulent pipe (Figure 9(c)), the pressure drop becomes relatively mild, demonstrating that even under turbulent conditions, large-diameter pipes are far more efficient in minimizing pressure loss. This confirms that pipe diameter remains the dominant controlling factor for pressure drop in turbulent internal flows [20].

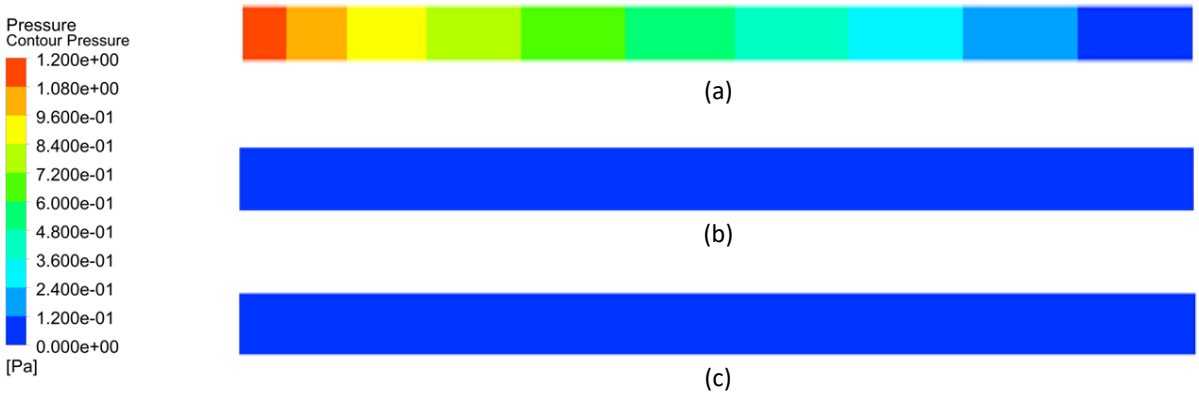

Fig. 8. Pressure contour for laminar flow in diameter pipe (a) 0.0254 m (b) 0.0508 m (c) 0.0762 m

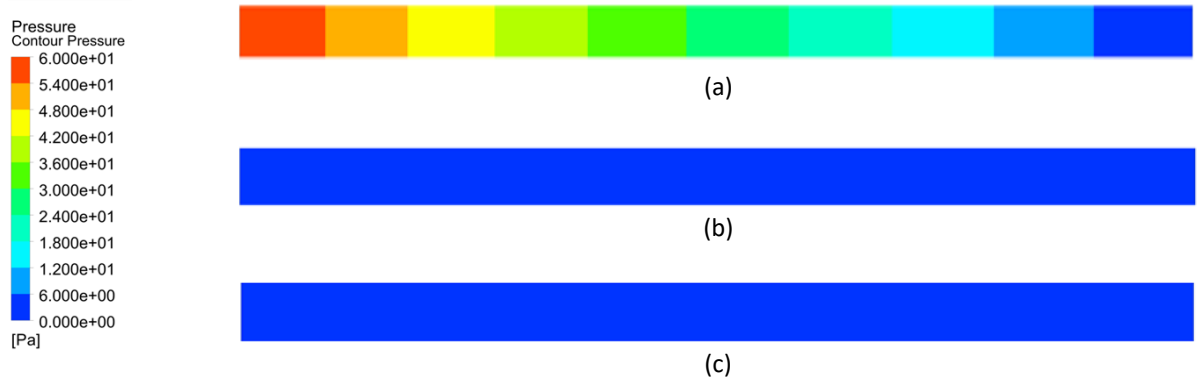

Fig. 9. Pressure contour for turbulent flow in diameter pipe (a) 0.0254 m (b) 0.0508 m (c) 0.0762 m pipe

3.4 Turbulent Kinetic Energy

Turbulent kinetic energy (TKE) represents the intensity of velocity fluctuations within a turbulent flow and is directly linked to turbulence production and energy dissipation. In this study, TKE contours are analysed only for turbulent flows using the realizable k–ε turbulence model at an inlet velocity of 0.3 m/s with 5% turbulence intensity. The TKE contours for all three pipe diameters are shown in Figure 10. In the 0.0254 m turbulent pipe (Figure 10(a)), the turbulent kinetic energy is highly concentrated near the pipe wall, indicating strong turbulence production caused by high wall shear stress. The small hydraulic diameter intensifies velocity gradients, leading to stronger turbulent eddies and higher energy dissipation. This behaviour closely matches the DNS observations of Yao *et*

al., [5], who reported that turbulence production is highest near the wall in small-diameter turbulent pipe flows.

Subsequently, in the 0.0508 m pipe (Figure 10(b)), the TKE level is noticeably reduced compared to the 0.0254 m case. Although turbulence remains present, the intensity of velocity fluctuations near the wall is weaker due to reduced wall confinement, which suppresses excessive turbulence generation. This trend is consistent with the RANS findings reported by Wu *et al.,* [21]. In the 0.0762 m turbulent pipe (Figure 10(c)), the turbulent kinetic energy reaches its lowest level among all cases, showing that the wider flow passage significantly weakens turbulent activity and energy dissipation. This confirms that under constant inlet velocity, turbulence intensity decreases as pipe diameter increases, which is a fundamental behaviour of turbulent internal flows [9,20]. Kinetic energy (TKE) represents the intensity of velocity fluctuations within a turbulent flow and is directly linked to turbulence production and energy dissipation. In this study, TKE contours are analysed only for turbulent flows using the realizable k–ε turbulence model at an inlet velocity of 0.3 m/s with 5% turbulence intensity. The TKE contours for all three pipe diameters are shown in Figure 10.

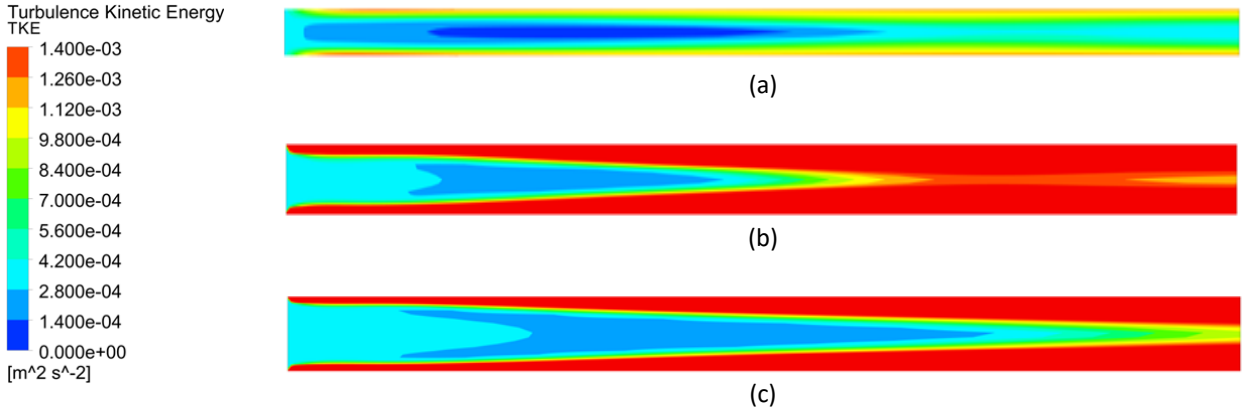

Fig. 10. Turbulence kinetic energy contour for turbulent flow in diameter pipe (a) 0.0254 m (b) 0.0508 m (c) 0.0762 m pipe

4. Conclusions

The CFD simulations performed in this study successfully demonstrated how pipe diameter and flow regime influence pressure drop in internal pipe flow. The results showed that the 0.0254 m pipe experienced the highest frictional losses in both laminar and turbulent conditions, with the turbulent case producing more than four times the laminar pressure drop due to increased wall shear and momentum mixing. In contrast, the 0.0254 m diameter 0.0508 m pipes exhibited very small pressure drops, remaining close to their laminar values even under turbulent modelling, indicating that larger diameters are far less sensitive to turbulence effects. These findings align with classical theory such as the Hagen–Poiseuille relation for laminar flow and with established turbulence behaviour reported in previous studies. Overall, the research objectives were achieved, confirming that smaller pipes are highly sensitive to flow regime while larger pipes maintain low pressure losses, and the CFD approach used provides reliable insight into diameter-dependent internal flow characteristics.

References

[1] Alawee, Wissam H., Yousef A. Almolhem, Badronnisa Yusuf, Thamer A. Mohammad, and Hayder A. Dhahad. "Variation of coefficient of friction and friction head losses along a pipe with multiple outlets." *Water* 12, no. 3 (2020): 844. https://doi.org/10.3390/w12030844

[2] Sahrane, Sara, and Slimane Niou. "Evaluating turbulence models for accurate thermo-fluid simulation in STHE with combined tube bundles." *Turkish Journal of Engineering* 9, no. 2 (2025): 258-271. https://doi.org/10.31127/tuje.1546393

[3] Cruz, Gonçalo G., Miguel AA Mendes, Jos MC Pereira, H. Santos, A. Nikulin, and Ana S. Moita. "Experimental and numerical characterization of single-phase pressure drop and heat transfer enhancement in helical corrugated tubes." *International Journal of Heat and Mass Transfer* 179 (2021): 121632. https://doi.org/10.1016/j.ijheatmasstransfer.2021.121632

[4] Sakamoto, Nobuaki, Takanori Hino, Hiroshi Kobayashi, and Kunihide Ohashi. "Parameter adaptation of k− ω SST turbulence model for improving resolution of moderately separated flows around 2D wing and 3D ship hulls via EnKF data assimilation." *Journal of Marine Science and Technology* 29, no. 4 (2024): 885-909. https://doi.org/10.1007/s00773-024-01026-y

[5] Yao, Jie, Saleh Rezaeiravesh, Philipp Schlatter, and Fazle Hussain. "Direct numerical simulations of turbulent pipe flow up to." *Journal of Fluid Mechanics* 956 (2023): A18. https://doi.org/10.1017/jfm.2022.1013

[6] Lahiri, Saptarshi Kumar, and Konstantin Volokh. "Transition from laminar to turbulent pipe flow as a process of growing material instabilities." *Results in Engineering* 23 (2024): 102535. https://doi.org/10.1016/j.rineng.2024.102535

[7] Yang, Qi, Jie Dong, Tongju Xing, Yi Zhang, Yong Guan, Xiaoli Liu, Ye Tian, and Peng Yu. "RANS-based modelling of turbulent flow in submarine pipe bends: Effect of computational mesh and turbulence modelling." *Journal of Marine Science and Engineering* 11, no. 2 (2023): 336. https://doi.org/10.3390/jmse11020336

[8] Di Nucci, Carmine, and Rafik Absi. "Comparison of Mean Properties of Turbulent Pipe and Channel Flows at Low-to-Moderate Reynolds Numbers." *Fluids* 8, no. 3 (2023): 97. https://doi.org/10.3390/fluids8030097

[9] De Maio, Mariangela, Beatrice Latini, Francesco Nasuti, and Sergio Pirozzoli. "Direct numerical simulation of turbulent flow in pipes with realistic large roughness at the wall." *Journal of Fluid Mechanics* 974 (2023): A40. https://doi.org/10.1017/jfm.2023.728

[10] Evran, Savaş, and Mustafa Kurt. "CFD and statistical analysis of flow mass ratios on temperature and pressure drops of double pipe heat exchanger." *International Journal of Low-Carbon Technologies* 18 (2023): 771-780. https://doi.org/10.1093/ijlct/ctad056

[11] Singh, Rajwinder, Jashanpreet Singh, Rahul Kumar, and Manish Gupta. "Computational fluid dynamics of flow over a cylindrical tube for steady and transient flow conditions." *International Journal on Interactive Design and Manufacturing (IJIDeM)* 19, no. 4 (2025): 2925-2935. https://doi.org/10.1007/s12008-024-01970-4

[12] Debtera, Baru, Venkatesa Prabhu Sundramurthy, and Ibsa Neme. "Computational fluid dynamics simulation and analysis of fluid flow in pipe: Effect of fluid viscosity." *Journal of Computational and Theoretical Nanoscience* 18, no. 3 (2021): 805-810. https://doi.org/10.2139/ssrn.4201717

[13] Aqeel, Muhammad, Huabing Wen, Zhao Xianrui, Zhang Ling, and Wei Wei. "Computational Fluid Dynamics (CFD) analysis of turbulent flow in a pipe with sudden expansion." *Sch J Eng Tech* 7 (2025): 424-435. https://doi.org/10.36347/sjet.2025.v13i07.001

[14] Ferreira, Pedro Leite, and Dídia Isabel Cameira Covas. "Mesh Sensitivity Analysis of Axisymmetric Models for Smooth–Turbulent Transient Flows." *Fluids* 9, no. 11 (2024): 268. https://doi.org/10.3390/fluids9110268

[15] Aycan, Osman, Adnan Topuz, and Lyes Kadem. "Evaluating uncertainties in CFD simulations of patient-specific aorta models using Grid Convergence Index method." *Mechanics Research Communications* 133 (2023): 104188. https://doi.org/10.1016/j.mechrescom.2023.104188

[16] Massaro, Daniele, Valerio Lupi, Adam Peplinski, and Philipp Schlatter. "Global stability of 180∘-bend pipe flow with mesh adaptivity." *Physical Review Fluids* 8, no. 11 (2023): 113903. https://doi.org/10.1103/PhysRevFluids.8.113903

[17] De Maio, Mariangela, Beatrice Latini, Francesco Nasuti, and Sergio Pirozzoli. "Direct numerical simulation of turbulent flow in pipes with realistic large roughness at the wall." *Journal of Fluid Mechanics* 974 (2023): A40. https://doi.org/10.1017/jfm.2023.728

[18] Yang, Qi, Jie Dong, Tongju Xing, Yi Zhang, Yong Guan, Xiaoli Liu, Ye Tian, and Peng Yu. "RANS-based modelling of turbulent flow in submarine pipe bends: Effect of computational mesh and turbulence modelling." *Journal of Marine Science and Engineering* 11, no. 2 (2023): 336. https://doi.org/10.3390/jmse11020336

[19] Tang, Ting-Ting, Fang-Qiu Li, Guang-Yao Wang, Jun Yan, and Zhao-Kuan Lu. "Comparative study of RANS models for simulating turbulent flow and heat transfer in corrugated pipes." *Water* 17, no. 17 (2025): 2649. https://doi.org/10.3390/w17172649

[20] Tummers, M. J., M. C. Schenker-van Rossum, R. Delfos, A. Twerda, and J. Westerweel. "Turbulent flow and friction in a pipe with repeated rectangular ribs." *Experiments in Fluids* 64, no. 10 (2023): 160. https://doi.org/10.1007/s00348-023-03685-w

[21] Wu, Jia-Bin, and Li Li. "Pressure–flow rate relationship and its polynomial expansion for laminar flow in a circular pipe based on exponential viscosity-pressure characteristics: An extension of classical Poiseuille's law." *Physics of Fluids* 35, no. 10 (2023). https://doi.org/10.1063/5.0172756

[22] Marpaung, Tulus Joseph Herianto, and Asima Manurung. "Computation analysis of flow in a round pipe with Navier-Stokes equations." *Journal of Research in Mathematics Trends and Technology* 4, no. 1 (2022): 1-14. https://doi.org/10.32734/jormtt.v4i1.15827